First Results from the Axion Dark-Matter Birefringent Cavity (ADBC) Experiment

Swadha Pandey,* Evan D. Hall, and Matthew Evans
LIGO Laboratory, Department of Physics, Massachusetts Institute of Technology, Cambridge, Massachusetts 02139, USA

(Received 22 April 2024; accepted 9 August 2024; published 11 September 2024)

Axions and axionlike particles are strongly motivated dark-matter candidates that are the subject of many current ground based dark-matter searches. We present first results from the Axion Dark-Matter Birefringent Cavity (ADBC) experiment, which is an optical bow-tie cavity probing the axion-induced birefringence of electromagnetic waves. Our experiment is the first optical axion detector that is tunable and quantum noise limited, making it sensitive to a wide range of axion masses. We have iteratively probed the axion mass ranges 40.9–43.3 neV/c^2, 49.3–50.6 neV/c^2, and 54.4–56.7 neV/c^2, and found no dark-matter signal. On average, we constrain the axionlike particle and photon coupling at the level $g_{a\gamma\gamma} \leq 1.9 \times 10^{-8}$ GeV^{-1}. We also present prospects for future axion dark-matter detection experiments using optical cavities.

DOI: 10.1103/PhysRevLett.133.111003

Introduction—It is now more than 40 years since the axion was proposed as a solution to the dark-matter problem [1–4]. Since then, searches for ultralight dark matter have expanded from the canonical axion into a more general class of pseudoscalar axionlike particles (ALPs), whose mass m_a could range from less than 10^{-20} eV/c^2 to 10^{-2} eV/c^2 [5].

To arrive at an observable signature of the ALP, we need some additional hypotheses about the expected properties of dark matter. Based on observations of Milky Way dynamics, the local density of dark matter (DM) is $\rho_{\mathrm{DM}} = 0.3$ GeV/cm^3; additionally, dark matter is expected to be cold, with a typical velocity $\sim 10^{-3}$ c [6] (cf. Ref. [7]). Together, these assumptions imply that for ALPs, the de Broglie wavelength is much larger than the typical interparticle spacing, and the dark matter is therefore well described as a classical field $a(t)$ oscillating near the ALP Compton frequency $\omega_a = m_a c^2/\hbar$ [8]. Under the standard model of the Milky Way's dark-matter halo, the occupation numbers follow a Maxwellian distribution in velocity [9,10] (cf. Ref. [11]), meaning that the ALP field is Doppler broadened, with a fractional full-width half-maximum linewidth $\Delta\omega_a/\omega_a \approx 3 \times 10^{-6}$ [10].

The Lagrangian for interaction between an ALP field and an electromagnetic field with Faraday tensor $F_{\mu\nu}$ is given by

$$\mathcal{L} \supset -\frac{1}{4} g_{a\gamma\gamma} a F_{\mu\nu} \tilde{F}^{\mu\nu}, \tag{1}$$

where $g_{a\gamma\gamma}$ represents the strength of the ALP-photon coupling. This modifies Maxwell's equations, leading to electromagnetic signatures that are, in principle, observable [12]. One such signature is that photon-coupled ALPs induce circular birefringence between left-hand and right-hand polarized (LCP, RCP) electromagnetic waves. For such a wave at an angular frequency ω_0 propagating through a classically oscillating ALP field $a(t)$ with Compton frequency $\omega_a \ll \omega_0$, the dispersion of the two circular polarization modes is [13]

$$c^2 k_{\mathrm{LCP,RCP}}(t)^2 - \omega_0^2 = \pm\omega_0 \frac{g_{a\gamma\gamma}}{m_a} \sqrt{\frac{2\hbar^3 \rho_{\mathrm{DM}}}{c}} \dot{a}(t), \tag{2}$$

with $k_{\mathrm{LCP,RCP}}$ being the wave number of the left- or right-handed electromagnetic mode. Searches for this signature have been proposed in the optical domain using resonant cavities [13–18], with initial experiments searching in the femto to picoelectronvolt range [19] and around 2 neV [20]. Searches for ALP-induced conversion between electromagnetic modes have also been proposed using superconducting rf cavities [21,22].

One of the experimental challenges of performing ALP searches with optical cavities is the ability to tune the cavity to search for ALPs of different masses. In this Letter we have, for the first time, demonstrated a technique to tune such a detector, paving the way for optical cavity based detection over a large range of ALP mass. We thus present a search for ALPs near 50 neV using a tunable and quantum-noise-limited birefringent optical cavity.

*Contact author: swadha@mit.edu

Experimental setup—Our experiment exploits the ALP-induced optical activity given by Eq. (2). If the ALP field $a(t)$ is quasisinusoidal, with a central frequency at the Compton frequency ω_a, then an $\hat{s}$-polarized electromagnetic wave with frequency ω_0 propagating through the ALP field will develop $\hat{p}$-polarized phase sidebands at frequency $\omega_0 \pm \omega_a$, i.e., at a distinct frequency and orthogonal polarization to the pump field. For propagation over a distance ℓ, the amplitude of the $E^{(\omega_0\pm\omega_a,\hat{p})}$ sidebands relative to the $E^{(\omega_0,\hat{s})}$ pump amplitude is given by [13]

$$\beta_\ell \equiv \frac{E^{(\omega_0\pm\omega_a,\hat{p})}}{E^{(\omega_0,\hat{s})}} = \frac{g_{a\gamma\gamma}}{2\omega_a}\sqrt{c^3\hbar\rho_{\rm DM}}(e^{\pm i\omega_a\ell/c}-1). \quad (3)$$

This polarimetric rotation is of order 10^{-16} for $g_{a\gamma\gamma} = 10^{-10}$ GeV^{-1} and $\ell = 1$ m. To enhance this small signal, we constructed a birefringent bow-tie cavity as depicted in Fig. 1, using a 1064 nm Nd:YAG laser as a pump. Our cavity is formed of four superpolished mirrors (labeled A, B, C, and D), with amplitude transmissivities t satisfying $t_{D,B}^{\hat{p},\hat{s}} \ll t_{A,C}^{\hat{p},\hat{s}}$. The mirror separations satisfy $L_{CA}, L_{DB} \ll L_{AD}, L_{BC}$, so that we take $L_{AD} \simeq L_{BC} \equiv L$. Because of non-normal incidence, the mirrors cause a phase splitting between $\hat{s}$- and $\hat{p}$-polarized light upon reflection. We have used mirrors such that this splitting is small for mirrors B and D, so the cumulative phase splitting Ψ per cavity round-trip is dominated by mirrors A and C. When the carrier mode $(\omega_0, \hat{s})$ is resonant in the cavity, the cavity will also be resonant for the mode $(\omega_0 + \omega_{\rm sp}, \hat{p})$, where $\omega_{\rm sp} = \Psi c/2L$ is the cavity frequency splitting between the $\hat{s}$ and $\hat{p}$ polarizations. Thus for $\omega_{\rm sp} = \omega_a$, the cavity is resonant for both the pump mode and one of the two ALP-generated signal modes.

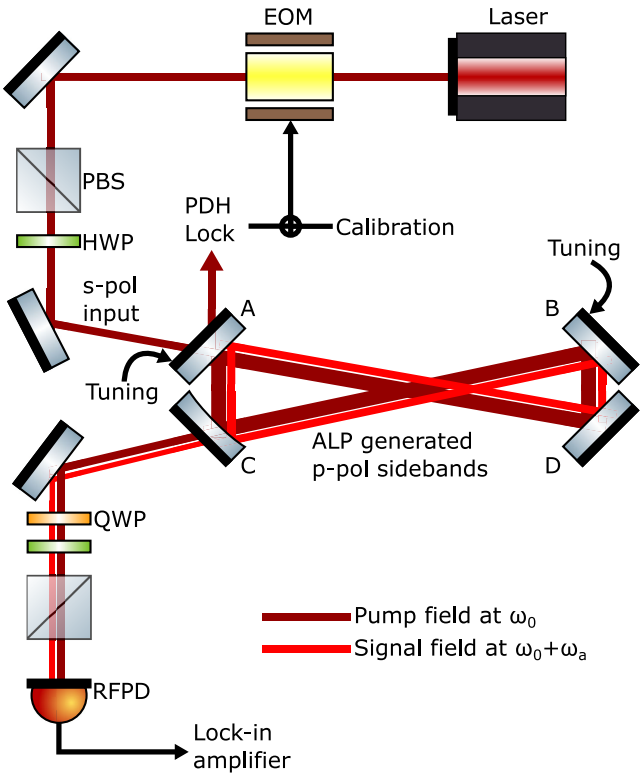

FIG. 1. Experimental setup: bow-tie cavity with A, D, B, C mirrors. $\hat{s}$-polarized pump field from a 1064 nm Nd:YAG laser enters the cavity at mirror A and is locked to the cavity using a Pound-Drever-Hall lock. $\hat{p}$-polarized sidebands generated by an axionlike particle (ALP) at the cavity splitting frequency $\omega_a = \omega_{\rm sp}$ are resonant in the cavity. Heterodyne readout is performed using pump and signal field transmitted at mirror C.

We lock our pump field to the cavity using a Pound-Drever-Hall (PDH) lock [23], with a loop bandwidth of 80 kHz. We characterize the cavity finesse in $\hat{s}$ by measuring the storage time [24], and in $\hat{p}$ by modulating the laser frequency to measure the cavity linewidth. Since mirror transmission varies markedly with angle of incidence, transmission values were measured *in situ* for each cavity mirror in both polarizations. The values for these parameters are given in Table I for our first dataset. The cavity sits inside a steel enclosure on a floating table.

To be sensitive to a wide range of ALP frequencies, we must tune the cavity splitting. We note that the reflection phase splitting at mirrors A and C is a sharp function of angle of incidence, and hence a small rotation of mirror B results in a significant shift in $\omega_{\rm sp}$. Mirror A is then rotated to close the cavity path again, and mirror C and the input optics are adjusted to maximize mode matching and hence intracavity pump power for the new configuration. This procedure is repeated each time to reach a new cavity splitting. For the first experimental run, the tuning process has been performed by manually adjusting the mirror angles, resulting in some gaps in the search mass regions. Automating the tuning process in future versions of the experiment will ensure smoother scanning of the ALP mass range.

TABLE I. Experimental parameters: round-trip cavity length $2L$, finesse $\mathcal{F}$, input power transmissivity $T_{\rm A}$, output power transmissivity $T_{\rm C}$, input power P_0, laser wavelength λ_0, and cavity splitting $\omega_{\rm sp}/2\pi$ for the first dataset. Where two values are given, the first refers to the $\hat{s}$-polarized pump mode, and the second refers to the $\hat{p}$-polarized signal mode. Values in parentheses denote uncertainties.

Parameter	Value		Unit
$2L$	4.70(1)		m
$\mathcal{F}$	7260(70)	212(1)	⋯
$T_{\rm A}$	$5.3(1)10^{-4}$	0.0150(8)	⋯
$T_{\rm C}$	$5.7(4)10^{-6}$	0.0130(3)	⋯
P_0	0.8		W
λ_0	1064		nm
$\omega_{\rm sp}/2\pi$	10.03		MHz

At the transmission of mirror C, we perform a polarimetric heterodyne readout. We use a quarter-wave plate to shift the signal modes from the phase quadrature to the amplitude quadrature relative to the pump field. We then use a half-wave plate to project some of the transmitted pump field onto the same polarization state as the transmitted signal field. Together, these two wave plates enable the production of an optical beat note at $\omega_{\rm sp}$ if ALPs are present. To sense this beat note, we use an rf photodiode with a bandwidth of 125 MHz. We then send the ac output of the photodiode to a lock-in amplifier, where we demodulate the signal at the cavity splitting $\omega_{\rm sp}$ over the signal mode cavity bandwidth, which is ∼300 kHz.

For a photon shot noise limited measurement, we calculate the amplitude signal-to-noise ratio [25]

$$\mathrm{SNR} = \frac{\epsilon_{\rm ro} g_{a\gamma\gamma}\sqrt{2P^{\hat{s}}_{\rm cav}\rho_{\rm DM}\hbar c t_C^{\hat{p}}}\mathcal{F}_p L}{\sqrt{\hbar\omega_0\pi}} \times \left|\sin c\left(\frac{\omega_a L}{c}\right)\right|(\tau T)^{1/4}, \quad (4)$$

where $P^{\hat{s}}_{\rm cav}$ is the intracavity pump power, T is the integration time, $\tau = 1/\Delta\omega_a$ is the coherence time of the ALP field, $\mathcal{F}$ is the cavity finesse, $t_{\rm C}^{\hat{p}}$ is the amplitude transmissivity of mirror C for the $\hat{p}$ polarization, and $\epsilon_{\rm ro}$ accounts for readout inefficiencies.

Calibration—To find the cavity splitting $\omega_{\rm sp}$ for a given cavity configuration, we send linearly polarized light into the cavity at ∼30° relative to its eigenaxis and then lock the $(\omega_0, \hat{s})$ mode to the cavity. We then drive an electro-optic modulator to generate $\hat{p}$ phase sidebands, one of which resonates when the sideband frequency matches $\omega_{\rm sp}$; this appears as a beat note at the readout photodiode.

To calibrate the noise floor of our apparatus, we calculate the strength of signal produced by a phase fluctuation that mimics the axion background. For a polarization rotation of $\beta_{2L}(\omega)$ over a single cavity round trip [Eq. (3)], the demodulated ac power measured at the readout photodiode is

$$P_{\rm ac}(\omega) = 2\sqrt{P_{\rm lo}P_0}\mathcal{F}_s\mathcal{F}_p\beta_{2L}(\omega)t_C^{\hat{p}}t_A^{\hat{s}}\frac{\epsilon_{\rm ro}\epsilon_{\rm inj}}{\pi^2}|C^{\hat{p}}(\omega)|, \quad (5)$$

where $C(\omega)$ is the normalized cavity amplitude transfer function, and $\epsilon_{\rm inj}$ accounts for injection inefficiencies (e.g., due to mode mismatch). We measure the amplitude spectral density at the rf photodiode, referred to intracavity phase $\beta(\omega)$ using Eq. (5) and our measured values of the finesses and transmissivities [25]. We infer an intracavity phase sensitivity of 1×10^{-12} rad/$\sqrt{\rm Hz}$, dominated by photon shot noise and with a −20 dB contribution from electronics noise.

Data taking and analysis—We took data in five discrete searches over the frequency range 9.88–13.69 MHz, with each dataset having a bandwidth of 300 kHz. Each measurement was taken for 3 h, with the data immediately demodulated at the cavity splitting frequency $\omega_{\rm sp}$, Fourier transformed, and accumulated into a power spectral density (PSD) estimate, with $N \sim 47\,000$ averages. An example dataset is shown in Fig. 2.

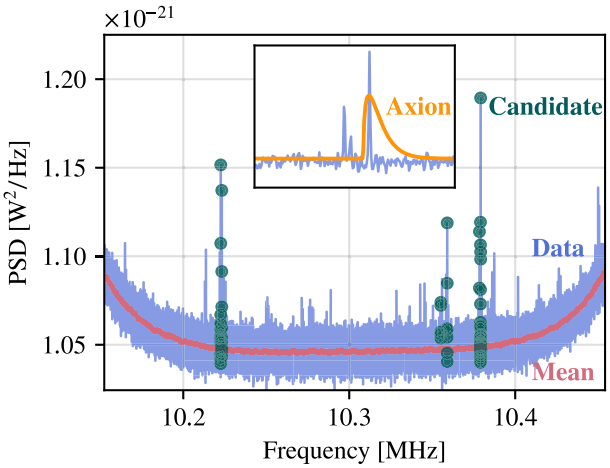

FIG. 2. Mean-averaged PSD data (blue), neighboring-bin running median to estimate the mean (pink), and points that lie above the detection threshold (green) for the second dataset. We also show a portion of the data overlayed with the expected axion line shape (orange), where it can be seen that the data peak is much narrower.

For each dataset, we perform a search for an ALP signal in the PSD data. A PSD estimate $S(\omega)$ resulting from N mean-averaged periodograms converges to a Gaussian, with probability density

$$P[S(\omega)] = \sqrt{\frac{N}{2\pi}}\frac{1}{\lambda(\omega)}\exp\left\{-\frac{[S(\omega)-\lambda(\omega)]^2}{2\lambda(\omega)^2/N}\right\}, \quad (6)$$

with $\lambda(\omega)$ representing the underlying true value of the PSD. For the case of no ALP signal i.e., the null hypothesis $\mathcal{H}_0$, the value of $\lambda(\omega)$ is just given by the detector noise PSD, which we call $\lambda_0(\omega)$. We infer $\lambda_0(\omega)$ using a running median of the neighboring 500 bins in the data. Since an axion signal is expected to be ∼10 bins wide, this gives us a background-only estimate.

In the presence of an ALP at ω_a, the ALP signal would have a power spectral density $\Gamma_{\omega_a}(\omega)F_{\omega_a}(\omega)$, where $F_{\omega_a}(\omega)$ is the ALP line shape [10], and $\Gamma_{\omega_a}(\omega) \propto g^2_{a\gamma\gamma}$. Thus, the total fluctuation in the detector has PSD

$$\lambda(\omega) = \lambda_0(\omega) + \Gamma_{\omega_a}(\omega)F_{\omega_a}(\omega). \quad (7)$$

For each potential ALP frequency, we construct an optimal test statistic,

$$Y(\omega) = \left(\sum_{\omega'} \frac{F_\omega(\omega')^2}{\lambda_0(\omega')^2}\right)^{-1} \sum_{\omega'} \frac{F_\omega(\omega')}{\lambda_0(\omega')^2} [S(\omega') - \lambda_0(\omega')], \tag{8}$$

with uncertainty $\sigma_Y(\omega) = [N \sum_{\omega'} F_\omega(\omega')^2/\lambda_0(\omega')^2]^{-1/2}$. Under the null hypothesis $\mathcal{H}_0$, $Y(\omega)/\sigma_Y(\omega)$ follows the standard normal distribution; otherwise, if an ALP is present with mass m_a and coupling $g_{a\gamma\gamma}$, then $Y(\omega)$ converges to $\Gamma_{\omega_a}(\omega)$. To reject $\mathcal{H}_0$ at the 5σ level, we would need a nonzero value of Y with an overall significance $\alpha = 2.9 \times 10^{-7}$. We therefore seek a threshold value $Y_*^{(n)}(\omega)$ satisfying

$$P(Y(\omega) > Y_*^{(n)}(\omega)|\mathcal{H}_0) = \alpha/n, \tag{9}$$

with n being the number of independent tests on the data [26, §10.7], i.e., the total bandwidth of our data divided by the ALP linewidth. For our data, $n = 8287$ and hence $Y_*^{(n)}(\omega) = 6.5\sigma_Y(\omega)$. We search for any data with $Y(\omega) > Y_*^{(n)}(\omega)$, and find tens to hundreds of such candidate points per dataset. This is shown in Fig. 2 for dataset 2. We now use our knowledge of the fractional full-width half-maximum linewidth of the ALP signal, $\Delta\omega_a/\omega_a \approx 3 \times 10^{-6}$ [10]. To each candidate we fit a Lorentzian line shape via least squares regression and find that no candidate has a linewidth within a factor of 2 of the expected ALP linewidth (most of the lines are found to be too narrow). We therefore reject all candidates and conclude that no ALP signal is present in the data.

We proceed to set upper bounds on $g_{a\gamma\gamma}$ at ω at 95% confidence by using the distribution of $Y(\omega)$ under $\mathcal{H}_1(g_{a\gamma\gamma}^{95\%}, \omega_a = \omega)$, the hypothesis for the existence of an ALP field with rest-frame Compton frequency $\omega_a = \omega$ and coupling strength $g_{a\gamma\gamma}^{95\%}$. This distribution is normal with

$$P(Y(\omega)|\mathcal{H}_1(g_{a\gamma\gamma}^{95\%}, \omega_a = \omega)) = \mathcal{N}(\Gamma_{\omega_a=\omega}(\omega), \sigma_Y(\omega)^2). \tag{10}$$

Since $Y(\omega)$ can take negative values, we use the Feldman-Cousins approach [27] to ensure non-negative confidence intervals. The upper limits thus obtained from our data are shown in Fig. 3 for the five datasets. The average sensitivity we have achieved is $g_{a\gamma\gamma}^{95\%} \leq 1.9 \times 10^{-8}$ GeV^{-1} over the probed frequency range.

Appraisal and future upgrades—We have performed an ALP dark-matter search using a 5 m optical bow-tie cavity over five different ALP masses in the range 40.9–56.7 neV/c^2, corresponding to an ALP Compton frequency 9.88–13.69 MHz. Each search had a sensitivity band of 300 kHz and we have probed the ALP-photon coupling at an average sensitivity of $g_{a\gamma\gamma}^{95\%} \leq 1.9 \times 10^{-8}$ GeV^{-1} over all datasets. In this process, we have demonstrated for the first time an optical polarimetry based ALP detector whose search range has been enhanced by frequency tunability.

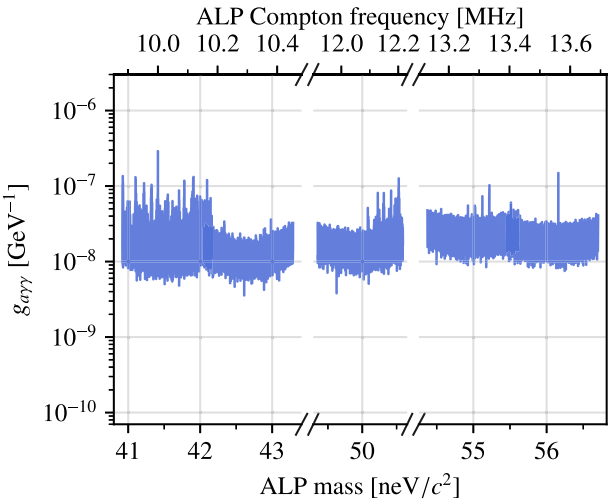

FIG. 3. 95% upper limit on $g_{a\gamma\gamma}$ placed by the first run of the ADBC experiment. We have bounds from five datasets over axion frequency ranges 9.88–10.45 MHz, 11.92–12.22 MHz, and 13.12–13.69 MHz with an average sensitivity of 1.9×10^{-8} GeV^{-1}.

A direct upgrade to this experiment would involve higher intracavity power, lower mirror transmission, and building a longer cavity. To scan the entire free spectral range of the cavity using the demonstrated tuning method, mirrors with narrowly angular-dependent polarization phase shift could be engineered by, for example, inserting a half-wave etalon layer into a quarter-wave coating stack. For rotations of order 0.1° on a 10 cm scale optic, linear actuation of order 0.1 mm would be required, which could be accomplished with a magnetically actuated suspension system similar to gravitational-wave interferometers. A suspended system, in concert with optical wavefront sensing [28], could then be used to maintain beam alignment into and within the cavity while the angle of incidence on the mirrors is tuned. We have thus assumed that the time required to adjust the tuning and alignment would be negligible compared to the integration time at each data-taking step. To reach shot-noise-limited sensitivity in the kilohertz band and below, more aggressive vibrational isolation may be required. Projections for an upgrade with $P_{\text{cav}} = 1$ MW, $\mathcal{F}_p = 10^5$, and $L = 40$ m are shown in Fig. 4, assuming a total integration time $T_{\text{total}} = 1$ yr allocated equally among all the dwell frequencies.

Photon counting for ALP detection has been proposed as an alternative [38,39] to heterodyne readout, where phase information is sacrificed for enhanced sensitivity. In the optical domain, this involves filtering out the pump photons at the readout port and using a single photon detector to measure the presence of any signal photons exiting the

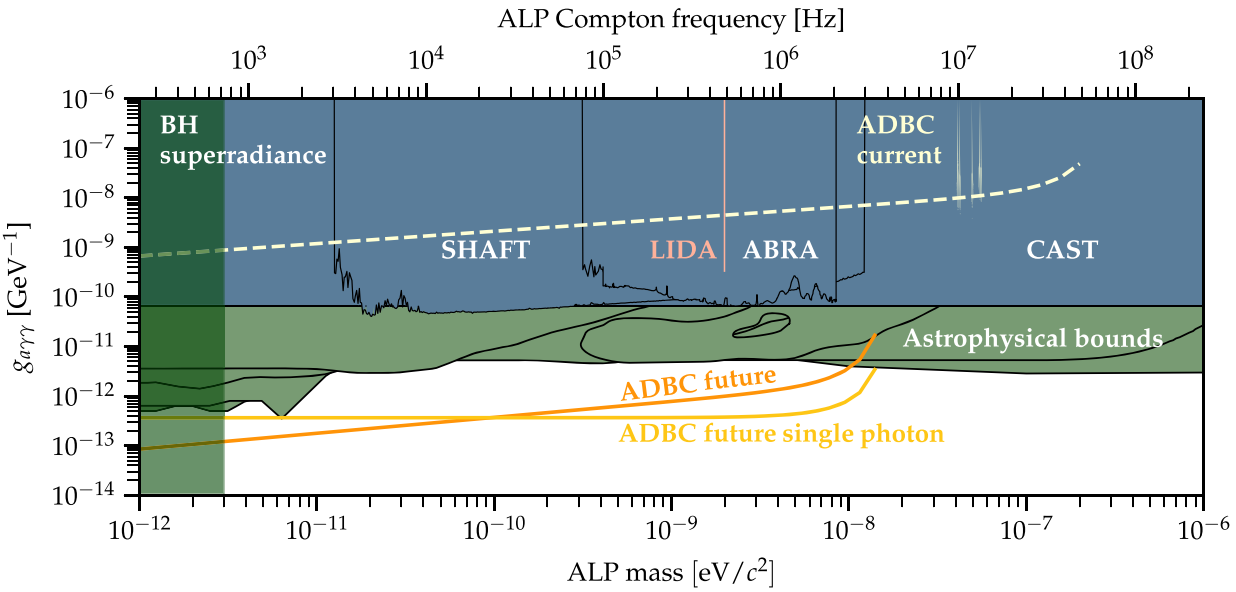

FIG. 4. Current bounds and future projections for implementations of optical ALP polarimetry. We show ADBC's current data run, along with a dashed line indicating the apparatus's current sensitivity if we performed a search over the full mass range. Sensitivities are also shown for a future ADBC upgrade still using heterodyne readout, as well as the same apparatus operated with single photon readout. Current bounds from other ALP polarimetry experiments include LIDA (shown in plot) and DANCE ($g_{a\gamma\gamma} \leq 8 \times 10^{-4}$ GeV^{-1} for 10^{-14} eV $< m_a c^2 < 10^{-13}$ eV). The blue regions show bounds from terrestrial ALP searches, in which we highlight the bounds from the solar axion search CAST [29], and the toroidal magnet searches ABRACADABRA [30] and SHAFT [31]. The green regions show various astrophysical constraints, particularly constraints from black hole superradiance [32–37].

cavity. Assuming Poissonian statistics for the photon fields, the SNR for such a measurement scheme is

$$\mathrm{SNR} = \frac{\dot{N}_p T}{\sqrt{[2(\dot{N}_s + \dot{N}_{\mathrm{dark}}) + \dot{N}_p]T}}, \tag{11}$$

where $\dot{N}_p$ and $\dot{N}_s$ are the rates of signal ($\hat{p}$) and pump ($\hat{s}$) photons reaching the single photon detector, and $\dot{N}_{\mathrm{dark}}$ is the dark count rate. To avoid being dominated by pump photon or dark noise at the detector, one has to make an optimistic projection of a dark count rate of 1 per hour and an extinction ratio of $\sim 10^{23}$ of pump to signal photons. One possible avenue includes a series of frequency-selective optical cavities located at the main cavity readout port, tuned to pass photons at the signal frequency and reject photons at the pump frequency [40]. The fact that the pump and signal modes are generated in orthogonal polarizations also enables some pump filtering via polarization-selective optics. Projections for the ADBC upgrade using this photon counting scheme are shown in Fig. 4, assuming the same time allocation strategy as the homodyne case.

Acknowledgments—This work was supported by the Charles E. Ross fund. S. P. was additionally supported by the Bruno Rossi Graduate Fellowship in Astrophysics, and E. D. H. was supported by the MathWorks, Inc. The authors thank Myron MacInnis for technical support, and Nancy Aggarwal, Rainer Weiss, and Lisa Barsotti for comments on the manuscript.

[1] J. Preskill, M. B. Wise, and F. Wilczek, Cosmology of the invisible axion, Phys. Lett. **120B**, 127 (1983).
[2] L. F. Abbott and P. Sikivie, A cosmological bound on the invisible axion, Phys. Lett. **120B**, 133 (1983).
[3] M. Dine and W. Fischler, The not so harmless axion, Phys. Lett. **120B**, 137 (1983).
[4] P. Sikivie, Invisible axion search methods, Rev. Mod. Phys. **93**, 015004 (2021).
[5] F. Chadha-Day, J. Ellis, and D. J. E. Marsh, Axion dark matter: What is it and why now?, Sci. Adv. **8**, abj3618 (2022).
[6] J. I. Read, The local dark matter density, J. Phys. G **41**, 063101 (2014).
[7] P. Salucci, F. Nesti, G. Gentile, and C. F. Martins, The dark matter density at the Sun's location, Astron. Astrophys. **523**, A83 (2010).
[8] L. Hui, Wave dark matter, Annu. Rev. Astron. Astrophys. **59**, 247 (2021).
[9] K. Freese, M. Lisanti, and C. Savage, Colloquium: Annual modulation of dark matter, Rev. Mod. Phys. **85**, 1561 (2013).
[10] A. Derevianko, Detecting dark-matter waves with a network of precision-measurement tools, Phys. Rev. A **97**, 042506 (2018).

[11] N. W. Evans, C. A. J. O'Hare, and C. McCabe, Refinement of the standard halo model for dark matter searches in light of the Gaia Sausage, Phys. Rev. D **99**, 023012 (2019).
[12] P. Sikivie, Experimental tests of the invisible axion, Phys. Rev. Lett. **51**, 1415 (1983); **52**, 695(E) (1984).
[13] Searching for axion dark matter with birefringent cavities, Phys. Rev. D **100**, 023548 (2019).
[14] W. DeRocco and A. Hook, Axion interferometry, Phys. Rev. D **98**, 035021 (2018).
[15] I. Obata, T. Fujita, and Y. Michimura, Optical ring cavity search for axion dark matter, Phys. Rev. Lett. **121**, 161301 (2018).
[16] D. Martynov and H. Miao, Quantum-enhanced interferometry for axion searches, Phys. Rev. D **101**, 095034 (2020).
[17] K. Nagano, T. Fujita, Y. Michimura, and I. Obata, Axion dark matter search with interferometric gravitational wave detectors, Phys. Rev. Lett. **123**, 111301 (2019).
[18] K. Nagano, H. Nakatsuka, S. Morisaki, T. Fujita, Y. Michimura, and I. Obata, Axion dark matter search using arm cavity transmitted beams of gravitational wave detectors, Phys. Rev. D **104**, 062008 (2021).
[19] Y. Oshima, H. Fujimoto, J. Kume, S. Morisaki, K. Nagano, T. Fujita, I. Obata, A. Nishizawa, Y. Michimura, and M. Ando, First results of axion dark matter search with DANCE, Phys. Rev. D **108**, 072005 (2023).
[20] J. Heinze, A. Gill, A. Dmitriev, J. Smetana, T. Yan, V. Boyer, D. Martynov, and M. Evans, First results of the laser-interferometric detector for axions (LIDA), Phys. Rev. Lett. **132**, 191002 (2024).
[21] P. Sikivie, Superconducting radio frequency cavities as axion dark matter detectors, arXiv:1009.0762.
[22] A. Berlin, R. T. D'Agnolo, S. A. R. Ellis, C. Nantista, J. Neilson, P. Schuster, S. Tantawi, N. Toro, and K. Zhou, Axion dark matter detection by superconducting resonant frequency conversion, J. High Energy Phys. 07 (2020) 088.
[23] R. W. P. Drever, J. L. Hall, F. V. Kowalski, J. Hough, G. M. Ford, A. J. Munley, and H. Ward, Laser phase and frequency stabilization using an optical resonator, Appl. Phys. B **31**, 97 (1983).
[24] T. Isogai, J. Miller, P. Kwee, L. Barsotti, and M. Evans, Loss in long-storage-time optical cavities, Opt. Express **21**, 30114 (2013).
[25] See Supplemental Material at http://link.aps.org/supplemental/10.1103/PhysRevLett.133.111003 for details on the ALP signature in a birefringent optical cavity, the calibration procedure, dataset parameters, single-photon readout sensitivity, and constraints from black hole superradiance.
[26] L. Wasserman, *All of Statistics* (Springer, New York, 2004).
[27] G. J. Feldman and R. D. Cousins, A unified approach to the classical statistical analysis of small signals, Phys. Rev. D **57**, 3873 (1998).
[28] E. Morrison, B. J. Meers, D. I. Robertson, and H. Ward, Automatic alignment of optical interferometers, Appl. Opt. **33**, 5041 (1994).
[29] S. Andriamonje *et al.* (CAST Collaboration), An improved limit on the axion-photon coupling from the CAST experiment, J. Cosmol. Astropart. Phys. 04 (2007) 010.
[30] C. P. Salemi *et al.*, Search for low-mass axion dark matter with ABRACADABRA-10 cm, Phys. Rev. Lett. **127**, 081801 (2021).
[31] A. V. Gramolin, D. Aybas, D. Johnson, J. Adam, and A. O. Sushkov, Search for axion-like dark matter with ferromagnets, Nat. Phys. **17**, 79 (2021).
[32] C. O'Hare, AxionLimits, https://cajohare.github.io/AxionLimits/ (2020).
[33] R. Brito, S. Ghosh, E. Barausse, E. Berti, V. Cardoso, I. Dvorkin, A. Klein, and P. Pani, Gravitational wave searches for ultralight bosons with LIGO and LISA, Phys. Rev. D **96**, 064050 (2017).
[34] R. Brito, S. Ghosh, E. Barausse, E. Berti, V. Cardoso, I. Dvorkin, A. Klein, and P. Pani, Stochastic and resolvable gravitational waves from ultralight bosons, Phys. Rev. Lett. **119**, 131101 (2017).
[35] K. K. Y. Ng, O. A. Hannuksela, S. Vitale, and T. G. F. Li, Searching for ultralight bosons within spin measurements of a population of binary black hole mergers, Phys. Rev. D **103**, 063010 (2021).
[36] C. Yuan, R. Brito, and V. Cardoso, Probing ultralight dark matter with future ground-based gravitational-wave detectors, Phys. Rev. D **104**, 044011 (2021).
[37] R. Brito and P. Pani, Black-Hole Superradiance: Searching for Ultralight Bosons with Gravitational Waves, edited by C. Bambi, S. Katsanevas, and K. D. Kokkotas (Springer, Singapore, 2021).
[38] S. K. Lamoreaux, K. A. van Bibber, K. W. Lehnert, and G. Carosi, Analysis of single-photon and linear amplifier detectors for microwave cavity dark matter axion searches, Phys. Rev. D **88**, 035020 (2013).
[39] H. Yu, O. Kwon, D. K. Namburi, R. H. Hadfield, H. Grote, and D. Martynov, Photon counting for axion interferometry, Phys. Rev. D **109**, 095042 (2024).
[40] L. McCuller, Single-photon signal sideband detection for high-power michelson interferometers, arXiv:2211.04016.